sciendo

POLISH MARITIME RESEARCH 1 (121) 2024 Vol. 31; pp. 35-42
10.2478/pomr-2024-0004

STUDY OF THE HYDRODYNAMIC CHARACTERISTICS OF ANTI-HEAVE DEVICES OF WIND TURBINE PLATFORMS AT DIFFERENT WATER DEPTHS

Hongyuan Xu [1]
Wei Wang [1, 2, 3] *
Yonghe Xie [1]*

[1] School of Naval Architecture and Maritime, Zhejiang Ocean University, Zhoushan , China
[2] School of Naval Architecture Ocean and Civil Engineering, Shanghai Jiaotong University, Shanghai, China
[3] Marine Design and Research Institute of China, Shanghai, China

* Corresponding authors: *wangwei1981@zjou.edu.cn (Wei Wang)*
xieyh@zjou.edu.cn (Yonghe Xie)

ABSTRACT

This paper focuses on the effect of water depth on the hydrodynamics of floating offshore wind turbines with open-hole anti-heave devices. The three-floating-body wind turbine platform is used as the primary research object in this paper. The effect of water depth on the reduction of the heave motion of a floating platform with anti-heave devices is systematically investigated through a series of experiments and numerical simulations. The results show high agreement between the test results and simulations, with larger values of heave motion in deep water. A wind turbine platform with anti-heave devices can effectively reduce the lifting and sinking motions when the wave period is large.

Keywords: anti-heave device; hydrodynamic analysis; different water depths

INTRODUCTION

Wind energy is a non-polluting, high retention and high potential renewable energy source, which has good prospects for development and application. Wind speed at sea is more stable and stronger than that on land because of its higher energy yield. By the end of 2020, offshore wind power's installed capacity surpassed 30 GW [1]. In areas of shallow water, there is considerable potential for bottom-fixed foundations, such as gravity and monopile types, which are limited to a maximum water depth of 15 and 30 m, respectively [2]. However, most of the offshore wind potential is located at sites with water depths of more than 60 m, where there is a greater advantage over the fixed type [3]. Floating offshore wind turbine (FOWT) platforms are more versatile in deep-sea applications [4]. In addition, semi-FOWTs can be efficiently used in a wide range of water depths [4]. Therefore, it is of great significance to study the platform's dynamic characteristics of semi-FOWTs at different water depths.

Many scholars have investigated the performance of FOWTs. Nematbakhsh et al. [6][7] investigated the dynamic response characteristics of TLP-type floating wind turbine systems and Spar-type floating wind turbine systems by using the CFD method and simplifying the turbines at a constant thrust. Hu et al. [8] investigated the dynamic response of a semi-submersible FOWT system under various excitations. The structural loading, in the case of emergency shutdown, has a stronger dynamic response. Abou-Rayan et al. [9] investigated the dynamic responses of triangular, square and pentagonal TLP configurations under multidirectional regular and random waves. Barrera et al. [10] explored the role of spectral wave characteristics and wave time histories in estimating extreme mooring loads for a floating offshore wind turbine. Zhao et al. [11] investigated the analysis of a kinematic fully-coupled time-domain simulation of a DTU10MW, comparing the motion response of DTU10MW with NREL5MW. The conclusions showed that the wind and waves had a more pronounced excitation effect on the DTU10MW wind turbine. Alkarem

et al. [12] investigated the effect of wave irregularities on the hydrodynamic response of a floating offshore wind turbine for FOWT at different water depths. Bae et al. [13] combined CHARM3D and FAST software to calculate the TPL floating wind turbine under different operating conditions and operating at water depths of 80 m and 200 m, carrying out numerical simulations in time domain analyses. Bayati et al. [14] analysed the effects of water depth on a semi-submersible type FOWT, where the water depth ranged from 30-200 m. It is claimed that water depths influence heave motion more than surge motion, when water depth decreases from 200 m to 30 m. Chen et al. [15] analysed the motion response of a wind turbine support platform, considering water depth effects. It is claimed that the effects of water depth mainly happen at shallower water depths. From a structural safety point of view, water depth effects need to be considered during the design process and the motion analysis of floating wind turbines. Le C et al. [16] proposed a new submerged offshore wind turbine aimed at operating in intermediate water depths between 20 and 200 m. Feasibility studies concerned different environmental conditions, tether length, tether pretension, and tether failure scenarios. Zhang et al. [17] studied the fully coupled analysis of the V-shaped floating wind turbine platform at different water depths; the mooring tension characteristics were analysed under different load conditions, yielding possible mooring schemes for different water depths. Studies have shown that surge, heave, and pitch motions are more stable at medium water depths. Lin [18] conducted a study of the impact of water depth (ranging from 200-300 m) on the performance of a floating offshore wind turbine. The results indicated that, as the water depth increases, the platform's heave motion tends to noticeably increase with mooring configuration.

In the design of FOWTs, water depth is considered as a design factor that must be addressed. In most of the research into reducing platform motion for improved stability, most of the tests are only conducted for a single water depth, ignoring the effect of water depth on platform motion. The 'deepCwind' platform base is taken as the research object in this paper. The hydrodynamic performance of a model with a chamfered perforated anti-heave device is systematically investigated through experiments with different water depth variations. Then, the models tested are compared and validated by full-scale numerical simulations. Finally, the effect of water depth variation on the reduction of heave motion is analysed by numerical simulation.

TOWING TANK EXPERIMENT

FLOATING BODY WITH ANTI-HEAVE DEVICES

Heave plates have the advantage of increasing the damping and additional mass coefficients in floating platforms, which can effectively increase the resistance of the platform and enhance stability. Wang et al. [19] studied the effect of opening holes on the pendulum plate, with chamfering angles of the holes from 0-35°, through a large number of experiments and numerical simulations. Among these, the 35° chamfered holes of the three-floating-body wind turbine platforms have the best effect on heave reduction. This paper selected a baseline offshore wind turbine designed by NREL 5 MW [20]. The data for the floating wind turbine platform with anti-heave devices are shown in Table 1. The single pontoon model, cross-section of the anti-heave device, and model of the platform with an anti-heave device are shown in Fig. 1.

Tab. 1 Overall parameters of floating offshore wind turbine

Parameters of wind turbine	Values
Rated power [MW]	5
Rotor diameter [m]	126
Cut in/Rated wind speed [m/s]	3/11.4
Cut in/Rated rotor speed [rpm]	6.9/12.1
Parameters of single floating body	**Values**
Height [m]	32
Diameter [m]	12
Diameter of anti-heave device [m]	24
Height of central column [m]	6
Number of perforations	10
Chamfer angle [deg]	35
Overall parameter	**Values**
Total mass [kg]	1.37×10^7

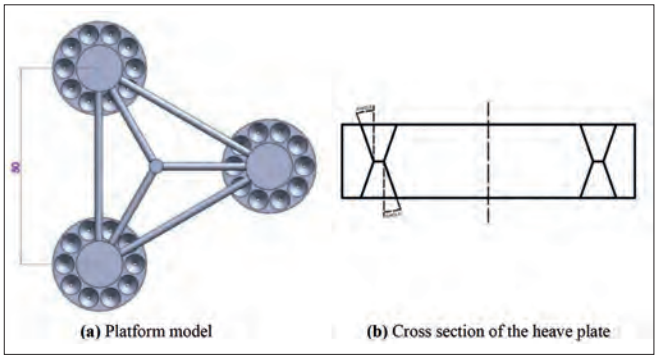

Fig 1. Anti heave device model

DESIGN OF EXPERIMENTS

Selection of scale ratio

According to the purpose of the test and the overall response characteristics of the floating wind turbine, it is necessary to satisfy the geometric similarity, kinematic similarity, and dynamic similarity [22]. At the same time according to the aerodynamic properties of the blade rotation, the TSR (tip speed ratio) was ensured to be similar [23]. In order to achieve similar overall load and wind turbine rotational effects, similar criteria were used in the equations:

$$\frac{L_S}{L_m} = \lambda \tag{1}$$

$$\frac{V_m}{\sqrt{gL_m}} = \frac{V_S}{\sqrt{gL_S}} \tag{2}$$

$$V_S = \lambda^{\frac{1}{2}} V_m \quad (3)$$

$$R_{TS} = \frac{\Omega_S R_S}{U_S} = \frac{\Omega_m R_m}{U_m} \quad (4)$$

$$R_S = \lambda^{-\frac{1}{2}} R_m \quad (5)$$

L is the length of the object feature, λ is the reduction ratio, V is the average velocity of the object with respect to the flow field, Ω is the rotational velocity of the impeller, R is the radius of the blades, and U is the average wind speed.

Based on the master scale, the scaling ratio was chosen as $\lambda = 60$. Table 2 shows the factors used to model the physical quantity conversion relationships:

Tab. 2. Relationship between model and actual physical quantity conversions

Property	Scale	Speed	Mass	Time	Frequency	Force	Rotor Speed	Inertia moment
Scaling factors	λ	$\lambda^{1/2}$	λ^{3}	$\lambda^{1/2}$	$\lambda^{-1/2}$	λ^{3}	$\lambda^{-1/2}$	λ^{4}

Experimental arrangement

Wave conditions were realised by the towing tank at Zhejiang Ocean University, which can control wave frequency and wave height to create stable regular waves.

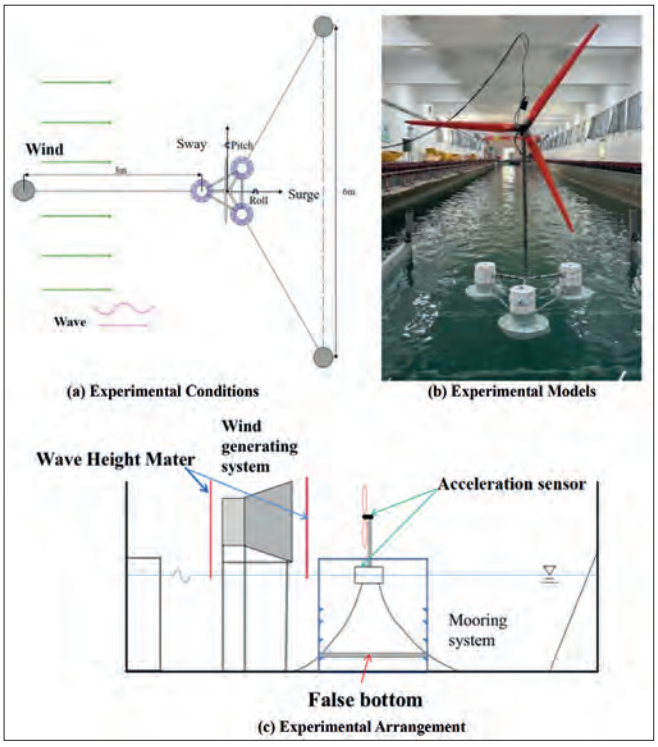

Fig. 2. Floating body model device and experimental arrangement diagram

The experiments included the acceleration of the platform motion, the 3-way accelerometer (Range: ±4g; Accuracy: 0.1%FS) at the top of the tower, by arranging the accelerometers, and the ULD2000 wave monitoring (Range: 0~0.5 m; Accuracy: 0.1%FS) and wind monitoring (Range: 0~40 m/s; Accuracy: ±0.5g + 2% FS). The pedestal model was obtained by 3D printing, which ensured smoothness and water tightness. The total mass of the model was 63.5 kg (including bulk) and the draft was 0.34 m. The mooring line (Fig. 2(a)) consisted of a 6.2 mm diameter steel wire rope (13.5 kg per 100 m) with a mass of 0.158 kg/m per unit length as the mooring cable; a 10 kg block was used in the towing tank as the mooring weight to fix the position of the mooring line. The experimental arrangement is shown in Fig. 2(b), consisting of a wind turbine blade and a float. The overall layout of the experiment and the environmental conditions are shown in Fig. 2 (c), which has three main components: the wave generation system, the wind generation system, and the wave dissipation system. The float model had a false bottom with adjustable depth, to control the water depth.

Due to the purpose of the experiment and the limited experimental conditions, this experiment was mainly carried out to study the heave motion response of the floating platform and the effect of the 35° chamfered holes on the heave motion of the anti-heave devices.

CONTENTS OF THE MODEL TEST

Hydrostatic decay tests

The hydrostatic decay test allows for obtaining the intrinsic period of the whole turbine system. For the hydrostatic free decay test, the upper turbine was set to stop and then adjusted so that the azimuth of one of the blades equals 0° (vertically upwards).

Model experiments under combined wind and wave action

According to the NERL-5MW wind turbine rating and the experimental wind and wave conditions, the scale conversion from Table 2 was used to select a constant wind speed of 1.30 m/s for this experiment; the waves were selected from the 15 sets of conditions, in Table 3, for the experimental conditions under combined wind and wave action.

Tab. 3. Experimental working conditions of the model under combined wind and wave action

Condition Number	Wave Frequency [Hz]	Wave Height [m]	Water Deep [m]
1	0.40	0.15	1.2
2	0.50	0.15	1.2
3	0.65	0.15	1.2
4	0.40	0.15	1.5
5	0.50	0.15	1.5
6	0.65	0.15	1.5
7	0.40	0.15	2.0
8	0.50	0.15	2.0
9	0.65	0.15	2.0
10	0.40	0.15	2.5
11	0.50	0.15	2.5
12	0.65	0.15	2.5
13	0.40	0.15	3.0
14	0.50	0.15	3.0
15	0.65	0.15	3.0

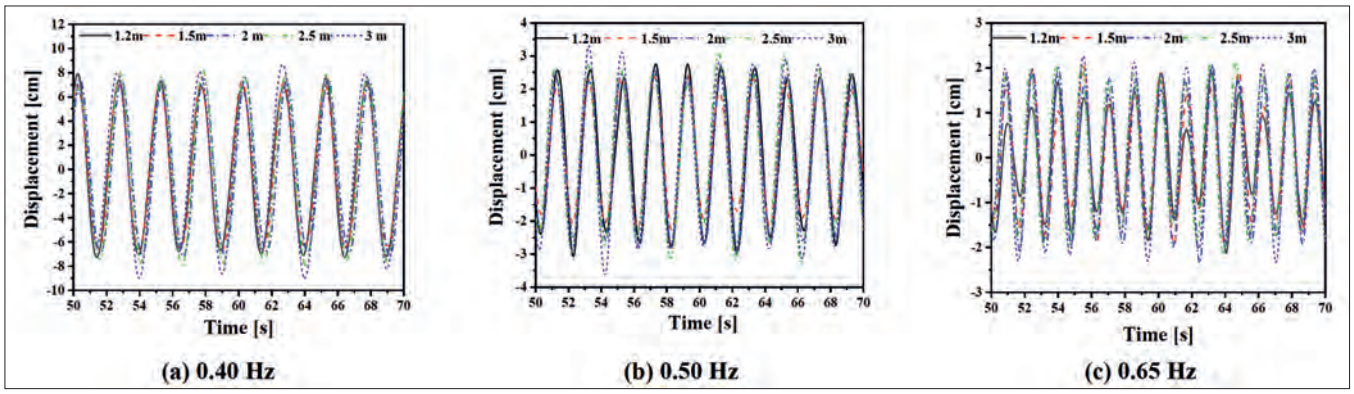

Fig. 3. Heave response of the floating body at different wave frequencies

TOWING TANK EXPERIMENT RESULTS

This experiment was conducted to measure the acceleration of a wind turbine platform with anti-heave devices. However, the actual process can interfere with the acceleration and the interference needs to be processed [24]. Integrating the processed acceleration twice gives the range of motion of the platform. The heave responses at different frequencies for each water depth are represented in Fig. 3.

The amplitude of the heave increases with the increase in water depth; the heave slowly increases when the water depth is 2-3 m.

NUMERICAL SIMULATION AND EXPERIMENTAL COMPARISON OF WIND TURBINE PLATFORMS AT DIFFERENT WATER DEPTHS

In this paper, a complete numerical simulation of a semi-submersible floating platform and NREL 5-MW wind turbine model was analysed using commercial CFD software STAR-CCM+ (17.02). The coupled response of the floating platform with anti-heave devices was specifically analysed under combined wind and wave conditions.

NUMERICAL METHODS

For transient, incompressible, and viscous fluids, the flow is governed by the continuity and Navier-Stokes equations:

$$\nabla \cdot u = 0 \tag{6}$$

$$\frac{\partial \rho U}{\partial t} + \nabla \cdot (\rho (U - U_g)\, U) = -\nabla P_d - g \cdot x \nabla \rho + \nabla \cdot (\mu_{eff} \nabla U) + (\nabla U) \cdot \nabla \mu_{eff} + f_\sigma \tag{7}$$

U and U_g represent the velocity of the flow field and grid nodes; P_d is the dynamic pressure of the low field (from subtracting the hydrostatic part from total pressure p); g is the gravity acceleration vector; r is the fluid density; e_{ff} denotes the effective dynamic viscosity of fluid, in which n and are the kinematic and eddy viscosity, respectively; and f_σ is a source term due to surface tension, which only takes effect at the free surface and equals zero elsewhere.

In order to capture the interface or free surface between air and water in a FOWT, the volume of fluid (VOF) method was used [25]. In the volumetric fluid method, the surface configuration was realised by the volume fraction, which varied between 0 and 1, depending on the percentage of the water phase in the cell volume. $\alpha = 1$ for the water cell, $\alpha = 0$ for the air cell and $0 < \alpha < 1$ for the air-water interface. The advection equation for a volume fraction is:

$$\frac{\partial \alpha}{\partial t} + \nabla \cdot (U\alpha) + \nabla \cdot [U_r \alpha\, (1-\alpha)] = 0 \tag{8}$$

A bounded compression technique was adopted to better capture the free surface, introducing an additional third compression term on the left-hand side of the transport equation, where U_r is a velocity field used to compress the interface.

COMPUTATIONAL DOMAINS AND PHYSICAL MODELS

The fluid domain range was selected to be -200 to 1000 m in the X direction, 200 m in the Y direction, and -160 to 300 m in the Z direction of the platform.

The front of the computational domain was set as the velocity inlet and the velocity was controlled by the velocity of the first-order VOF wave. The back of the computational domain was set as the pressure outlet and the pressure controlled by the hydrostatic pressure of the first-order VOF wave[26]. In addition, concerning the physical conditions of the model tested, a wave-damping zone was set up, considering the wave reflection near the outlet boundary; it minimised the effect of wave reflection on the far downstream outlet boundary[27].

The mooring system was set up in the form of three suspension chain lines, each with an angle of 120°, connected to three cable guide holes located at the bottom of the pontoon and a cable guide anchor located at the bottom of the computational domain[28].

MESH

The convergence of the numerical simulation was verified by comparing three different grid numbers: 1.31×10^7, 1.08×10^7, and 7.8×10^6. Fig. 4 represents the heave motion of the deepCwind turbine platform with different computational domain sizes under the same wave height and wave frequency, under the action of the floating-body heave.

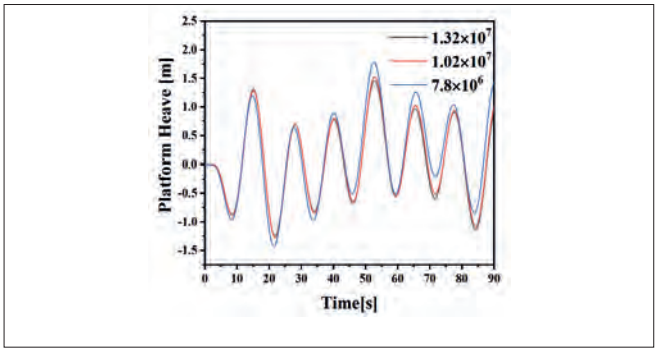

Fig. 4. Verification of the convergence of the calculation results by the number of grids

Comparing the three different calculation mesh quantities, the heave motion value of the three-floating-body wind turbine platform changes less when the calculation domain is small, and the Z-direction displacements of the DeepCwind platform are closer to each other as the calculation domain keeps increasing. Considering the number of grids, computational time consumption, and reliability of the results, 1.08×10^7 grids and 0.1 s time steps were selected for the related numerical analysis. The grid layout is shown in Fig. 5.

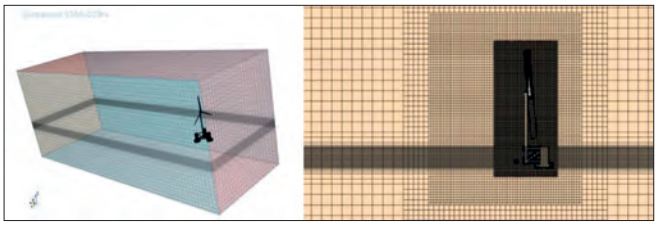

Fig. 5. Computational domain and mesh

RESULTS AND DISCUSSION

The main results discussed in this section include 'free decay' and 'kinematic response'. Numerical analyses were performed on the full-size model and the results scaled, as in Table 2.

COMPARISON OF HYDROSTATIC DECAY EXPERIMENTS

The free decay motion of heave and pitch is illustrated in Fig. 6. On the free decay curve, the time interval between two adjacent peaks or troughs is one oscillation period. The corresponding intrinsic period of the free decay motion can be obtained by randomly selecting multiple neighbouring peaks (troughs) and calculating the average value of multiple oscillation periods.

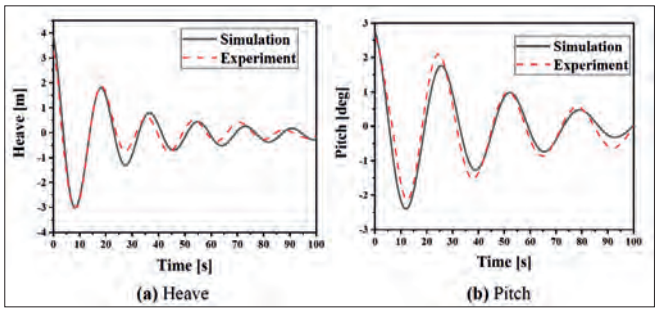

Fig. 6. Free decaying motion

Tab. 4. Natural periodicity of wind turbine platforms with damping devices

Parameters	Model Value [s]	Simulation Values [s]	Difference [%]
Heave period	16.78	17.67	5.0%
Pitch period	26.45	25.61	3.2%

The platform heave and pitch motions between hydrostatic attenuation test results and values were compared. The experimental and numerical simulation values differ between 5.0% and 3.2%. These discrepancies could arise from various sources, including model simplifications, scaling effects, and experimental errors.

COMPARISON OF NUMERICAL SIMULATION AND EXPERIMENTAL RESULTS

Numerical simulations of a real-scale wind turbine platform were carried out by experimental working conditions. The numerical simulation included the analysis of the water depth on the wind turbine platform with anti-heave devices and the original model [20]. The reliability of the numerical simulation was verified through experiments and the analysis of the heave motion in the model with anti-heave devices, as well as the original model.

By simulating the five water depths for the working conditions and comparing them with the experimental results, the time domain curves for different cases are shown in Fig. 7.

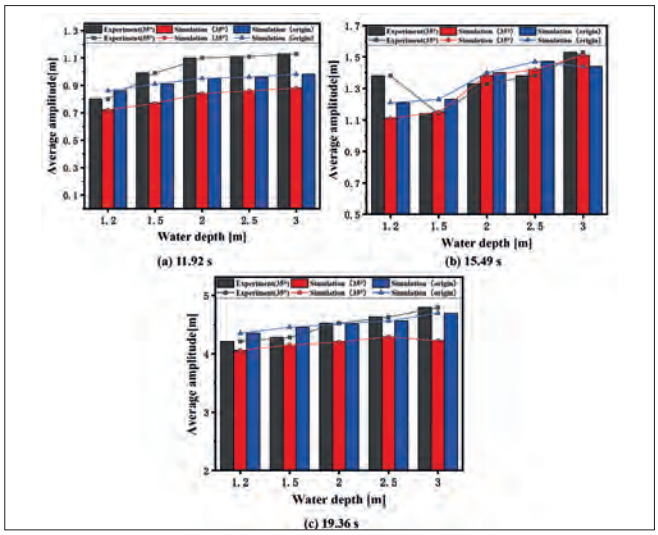

Fig. 7. Numerical and experimental results in the different water depth conditions.

Tab. 5. Summary of simulation and experimental results

Condition number	Frequencies[Hz]	Water depth [m]	Average amplitude [m]		
			Experiment (35°)	Simulation (35°)	Simulation (origin)
1	0.40	1.2	3.71	3.55	3.85
2	0.50	1.2	1.38	1.11	1.21
3	0.65	1.2	0.80	0.72	0.86
4	0.40	1.5	3.78	3.65	3.95
5	0.50	1.5	1.14	1.15	1.23
6	0.65	1.5	0.99	0.77	0.91
7	0.40	2.0	4.02	3.70	4.01
8	0.50	2.0	1.33	1.38	1.40
9	0.65	2.0	1.10	0.84	0.95
10	0.40	2.5	4.13	3.79	4.06
11	0.50	2.5	1.38	1.42	1.47
12	0.65	2.5	1.11	0.86	0.96
14	0.40	3.0	4.29	3.80	4.19
14	0.50	3.0	1.53	1.51	1.44
15	0.65	3.0	1.13	0.88	0.98

The numerical simulation data were converted to a particular scale and compared with the experimental data. As seen in Fig. 7, the numerical simulation and experimental results can maintain the same heave trend in the same cycle and the motion amplitude of the experiment is larger than that of the numerical simulation. It can be seen that, the larger the period, the better the match. At wave period 15.49 s, the difference between the experimental and simulated values for each water depth is minimal. The error may be due to the constraints of the pedestal in the numerical simulation, the difference in the conduit material, and the error of the experimental equipment when capturing the motion. The average amplitudes of the experimental and numerical simulation results are shown in Table 5.

As shown in Table 5, the average amplitude of the heave motion in the numerical simulation and testing kept the same change rule. For the same frequency, the deeper the water depth, the greater the amplitude of the floating body movement when the water depth position was more than 2 m (the actual value was 120 m). When the movement amplitude grows slowly and tends to be stable, at this time, the water depth tends towards the infinite; however, at the same water depth position, the wave period is large, the amplitude of the floating body movement increases, and the numerical simulation results are in better agreement with the experimental results. The anti-heave device with 35° chamfered holes has a similar change in the response of the heave motion to the original model. In most working conditions, the heave motion reduction effect of the 35° chamfered perforation model is obvious.

CONCLUSIONS

In this study, the experimental and numerical methods are used to investigate the kinematic response of a floating wind turbine platform with chamfered holes and anti-heave devices. The following conclusions were obtained by analysing the heave motion at different water depths and wave periods.

(1) When the water depth becomes deeper, the amplitude of the heave motion of the three-floating-body wind turbine platform increases. At depths greater than 120 m (deep water) the amplitude of the heave motion increases slowly and stabilises.
(2) The anti-heave effect of the three-floating-body wind turbine platform is affected by different waves. In most working conditions, the heave motion reduction effect of the wind turbine platform with anti-heave devices is obvious.
(3) The effect of heave reduction of the wind turbine platform with anti-heave devices is more evident when the water depth increases. The smaller the wave period, the more obvious the effects of the reducing heave.

ACKNOWLEDGEMENTS

This study was financially supported by "Pioneer" and "Leading Goose"R&D Program of Zhejiang (2022C03023), and the major research and development project of Daishan County Zhejiang Province (grant no. 202202).

REFERENCES

1. Counci, 'https://gwec.net/global-wind-report-2021', GLOBAL WIND REPORT. 2021.
2. G. Nagababu, S.S. Kachhwaha, and V. Savsani, 'Estimation of technical and economic potential of offshore wind along the coast of India', Energy. 2017, doi:10.1016/j.energy.2017.07.032.
3. A. Goupee, B. Koo, R. Kimbal, K. Lambrakos, and H.J. Dagher,

'Experimental Comparison of Three Floating Wind Turbine Concepts', International Conference on Ocean, Offshore and Arctic Engineering. 2014.

4. X. Wu, Y. Hu, Y. Li, J. Yang, L. Duan, T. Wang, and S. Liao, 'Foundations of offshore wind turbines: a review', Renew and Sustain. Energy Review. 2019, doi:10.1016/j.rser.2019.01.012.

5. Q. Cao, L. Xiao, Z. Chen, and M. Liu, 'An experimental study on dynamic behavior of a new concept of 10MW semi-submersible wind turbine', ISOPE International Ocean and Polar Engineering Conference. ISOPE. 2020.

6. A. Nematbakhsh, D.J. Olinge, and G. Tryggvason, 'A nonlinear computational model of floating wind turbines', Journal of Fluids Engineering. 2013, doi:10.1115/1.4025074.

7. A. Nematbakhsh, D.J. Olinge, and G. Tryggvason, 'A Nonlinear simulation of a spar buoy floating wind turbine under extreme ocean conditions', Journal of Renewable and Sustainable Energy. 2014, doi:10.1063/1.4880217.

8. Z. Hu, L. Li, J. Wang, Q. Hu, and M.C. Shen, 'Dynamic responses of a semi-type offshore floating wind turbine during normal state and emergency shutdown', China Ocean Engineering. 2016, doi:10.1007/s13344-016-0005-y.

9. A.M. Abou-Raya, N.N. Khali, and M.S. Afify, 'Dynamic behavior of TLP's supporting 5-MW wind turbines under multi-directional waves', Ocean Systems Engineering. 2016, doi:10.12989/ose.2016.6.2.203.

10. C. Barrera, I.J. Losad, R. Guanche, and L. Johanning, 'The influence of wave parameter definition over floating wind platform mooring systems under severe sea states', Ocean Engineering. 2019, doi:10.1016/j.oceaneng.2018.11.018.

11. Z. Zhao, W. Wang, W. Shi, and X. Li, 'Effects of second-order hydrodynamics on an ultra-large semi-submersible floating offshore wind turbine', Structures. 2020, doi:10.1016/j.istruc.2020.10.058.

12. Y.R. Alkarem and B.O. Ozbahceci, 'A complemental analysis of wave irregularity effect on the hydrodynamic responses of offshore wind turbines with the semi-submersible platform', Applied Ocean Research. 2021, doi:10.1016/j.apor.2021.102757.

13. Y.H. Bae, M.H. Kim, and Y.S. Shin, 'Rotor-floater-mooring coupled dynamic analysis of mini TLP-type offshore floating wind turbines', International Conference on Offshore Mechanics and Arctic Engineering, OMAE. 2010.

14. I. Bayati, S. Gueydon, and M. Belloli, 'Study of the effect of water depth on potential flow solution of the OC4 semi-submersible floating offshore wind turbine', Energy Procedia. 2015, doi:10.1016/j. egypro.2015.11.419.

15. X. Chen, H. Yu, W. Wang, and B. Wang, 'Analysis of Motion Response of Wind Turbine Platform Considering Different Heading Angles and Water Depth', 2nd International Conference on Sustainable Energy, Environment and Information Engineering (SEEIE). Atlantis Press. 2019.

16. C. Le, Y. Li, and H. Ding, 'Study on the coupled dynamic responses of a submerged floating wind turbine under different mooring conditions', Energies. 2019, doi:10.3390/en12030418.

17. L. Zhang, C. Michailides, Y. Wang, and W.Shi, 'Moderate water depth effects on the response of a floating wind turbine', Structures. 2020, doi:10.1016/j.istruc.2020.09.067.

18. Z. Lin, X. Liu, and S. Lotfian, 'Impacts of water depth increase on offshore floating wind turbine dynamics', Ocean Engineering. 2021, doi:10.1016/j.oceaneng.2021.108697.

19. W. Wei, Z. Chen, J. Panpan, L. Zhiqiang, and X. Yonghe, 'Numerical simulation and experimental study on perforated heave plate of a DeepCwind floating wind turbine platform', Ships and Offshore Structures. 2022, doi:10.1080/17445302.2022.2062157.

20. W. Wei, F. Sheming, Y. Yunxiang, Z. Cheng, X. Liqun, W. Guibiao and L. Zhiqiang. 'Study on the Influence of Chamfer Perforation on Heave and Pitch of a Single Floating Platform' Polish Maritime Research. 2023. doi:/10.2478/pomr-2023-0005

21. A. Robertson, J. Jonkman, M. Masciola, H. Song, A. Goupee, A. Coulling, and C. Luan, 'Definition of the semi-submersible floating system for phase II of OC4', National Renewable Energy Lab (NREL). Golden, CO (United States). 2014, doi:10.2172/1155123.

22. J. Chen, Z. Liu, Y. Song, Y. Peng, and J. Li, 'Experimental study on dynamic responses of a spar-type floating offshore wind turbine', Renewable Energy. 2022, doi:10.1016/j.renene.2022.06.149.

23. L. Meng, Y. He, Y. Zhao, T. Peng, and J. Yang, 'Experimental study on aerodynamic characteristics of the model wind rotor system and on characterization of a wind generation system', China Ocean Engineering. 2019, doi:10.1007/s13344-019-0014-8.

24. A. Kafeel, S. Aziz, M. Awais, M.A. Khan, K. Afaq, S.A. Idris, and S.M. Mostafa, 'An expert system for rotating machine fault detection using vibration signal analysis', Sensors. 2021, doi:10.3390/s21227587.

25. C.W. Hirt and B.D. Nichols, 'Volume of fluid (VOF) method for the dynamics of free boundaries', Journal of Computational Physics. 1981, doi:10.1016/0021-9991(81)90145-5.

26. T.T. Tran and D.H. Kim, 'A CFD study of coupled aerodynamic-hydrodynamic loads on a semi-submersible floating offshore wind turbine', Wind Energy. 2017, doi:10.1002/we.2145.

27. Y. Zhang and B. Kim, 'A fully coupled computational fluid dynamics method for analysis of semi-submersible floating offshore wind turbines under wind-wave excitation conditions based on OC5 data', Applied sciences. 2018, doi:10.3390/app8112314.

28. T.T. Tran and D.H. Kim, 'The coupled dynamic response computation for a semi-submersible platform of floating offshore wind turbine', Journal of wind engineering and industrial aerodynamics. 2015, doi:10.1016/j.jweia.2015.09.016.